

Dynamic Self-Repairing Hybrid Liquid-in-Solid Protective Barrier for Cementitious Materials

Gurminder K. Paink, Stefan Kolle, Duy Le, James C. Weaver, Jack Alvarenga, Onyemaechi Ahanotu, Joanna Aizenberg,* and Philseok Kim*



Cite This: *ACS Appl. Mater. Interfaces* 2020, 12, 31922–31932



Read Online

ACCESS |



Metrics & More



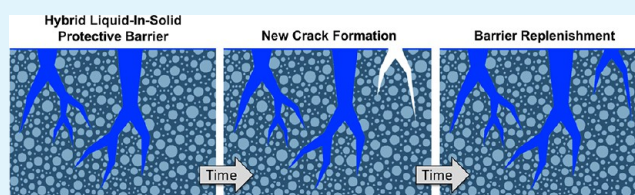
Article Recommendations



Supporting Information

ABSTRACT: Corrosion and surface fouling of structural materials, such as concrete, are persistent problems accelerating undesirable material degradation for many industries and infrastructures. To counteract these detrimental effects, protective coatings are frequently applied, but these solid-based coatings can degrade or become mechanically damaged over time. Such irreversible and irreparable damage on solid-based protective coatings expose underlying surfaces and bulk materials to adverse environmental stresses leading to subsequent fouling and degradation. We introduce a new concept of a hybrid liquid-in-solid protective barrier (LIB) to overcome the limitations of traditional protective coatings with broad applicability to structural materials. Through optimization of capillary forces and reduction of the interfacial energy between an upper mobile liquid and a lower immobile solid phase, a stable liquid-based protective layer is created. This provides a persistent self-repairing barrier against the infiltration of moisture and salt, in addition to omniphobic surface properties. As a model experimental test bed, we applied this concept to cementitious materials, which are commonly used as binders in concrete, and investigated how the mobile liquid phase embedded within a porous solid support contributes to the material's barrier protection and antifouling properties. Using industry standard test methods for acid resistance, chloride-ion penetrability, freeze–thaw cyclability, and mechanical durability, we demonstrate that LIBs exhibit significantly reduced water absorption and ion penetrability, improved repellency against various nonaqueous liquids, and resistance to corrosion while maintaining their required mechanical performance as structural materials.

KEYWORDS: barrier protection, hybrid liquid–solid materials, functional coatings, antifouling, anticorrosion



1. INTRODUCTION

Concrete is a ubiquitous building material that has been used for millennia, from construction of the Roman Colosseum to modern-day skyscrapers and monuments. The widespread use of concrete is attributed to its low cost and structural stability. In addition to filler materials such as pebbles, flyash, slag, and other additives, a key component of concrete is the cement binder, which when mixed with water forms a paste and over time forms a rigid porous structure via hydration.¹ Today, Portland cement (PC) is the most common type of cement with an annual consumption in excess of 4 billion metric tons. However, alternate cementitious materials such as geopolymers (GP) have recently garnered interest as they provide comparable mechanical properties to PC with a lower carbon footprint.^{2–4}

The surface and bulk of cementitious materials are highly porous and hydrophilic by nature, rendering them prone to absorption of moisture and permeation of vapors, particularly atmospheric precipitation and salt water from marine environments. As a result, undesirable ions and microorganisms can migrate through the concrete and accelerate structural degradation through various mechanisms, including steel corrosion and water expansion.^{5–8} Chloride ions are among the most destructive contaminants, promoting the corrosion of

steel reinforcements in concrete by catalyzing the formation of iron oxides in the presence of water.^{9–11} These iron oxides further promote the accumulation of moisture. In cold weather, entrapped water can expand up to 9 vol %, resulting in the buildup of mechanical stress in the concrete over time.⁹ Continuous stress due to seasonal change in combination with the ingress of ions inevitably leads to embrittlement and cracking of the concrete as well as degradation of the reinforcements.⁹

Currently, there are a number of different methods employed to increase the service life of concrete by reducing its permeability (Figure 1a) including (i) solid material coatings and sealants which provide a physical barrier, (ii) pore blockers which react with residual soluble concrete components to form insoluble products, and (iii) pore liners which increase the hydrophobicity of the cracked surfaces.^{11,12} Beyond these

Received: April 6, 2020

Accepted: June 12, 2020

Published: June 12, 2020



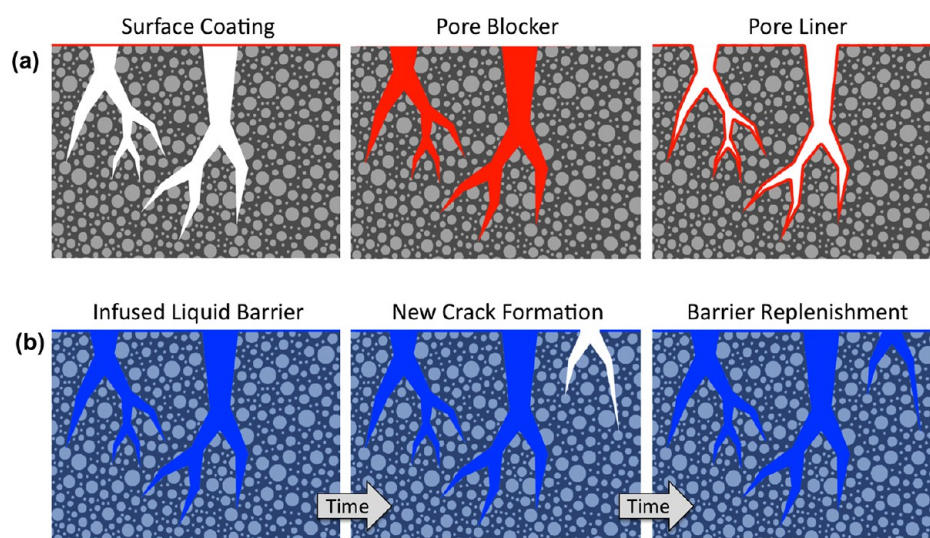


Figure 1. Schematic presentations of (a) the existing conventional solid-based protective coating technology and (b) the mechanism of action of a hybrid liquid-in-solid protective barrier (LIB) technology. Note how the liquid component migrates to block both existing and newly formed cracks.

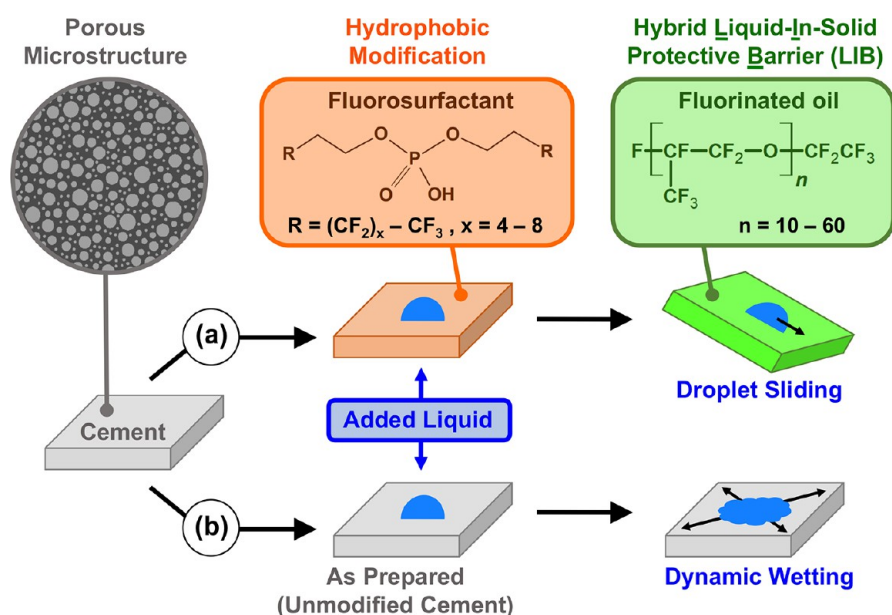


Figure 2. Schematic of the procedure used to introduce LIB to a cementitious material. (a) Porous cement was chemically functionalized using a fluoroaliphatic phosphate ester (fluorosurfactant, FS) and then infused with a chemically compatible liquid (fluorinated oil). After application of LIB, liquid contaminants immiscible with the fluorinated oil are blocked from entering the cement. (b) Liquid contaminants dynamically wet and readily absorb into the untreated Portland cement.

traditional industrial methods, new strategies such as superhydrophobic coatings and the incorporation of nanomaterials have been introduced to address these concerns.^{13–16} Despite the benefits of these solutions, the longevity of solid-based coatings is limited as the coatings themselves are susceptible to formation of new cracks and other irreparable surface defects via mechanical, chemical, and thermal challenges.¹¹ When a new defect or surface opening is formed on these solid-based coatings, moisture and other contaminants can then permeate and accelerate the degradation of underlying structural materials.

Several studies have demonstrated the utility of liquids as a component in designing self-replenishing and self-healing surfaces on porous or textured materials as well as polymers.^{17–28} The ability of the liquid component to

reconfigure on the surface has shown great promise in enhancing the resistance of engineered surfaces against ice formation,^{29–40} bacterial and fungal growth,^{41–52} and other forms of fouling.^{53–60} We anticipate that a similar principle can be applied to a bulk porous material, where a liquid component migrating in the bulk can provide excellent barrier properties to protect the underlying solid. Compared to a solid-based barrier coating, which generally lacks the ability to self-repair (once damaged) and cannot effectively block permeating liquids or vapors, a mobile liquid-based barrier can reconfigure to fill new voids, cracks, and conduits as they are formed, thus functioning as an effective dynamic barrier layer (Figure 1b).¹⁸

In the present study, we describe the implementation of a hybrid liquid-in-solid protective barrier (LIB) integrated within conventional cementitious materials and demonstrate that this

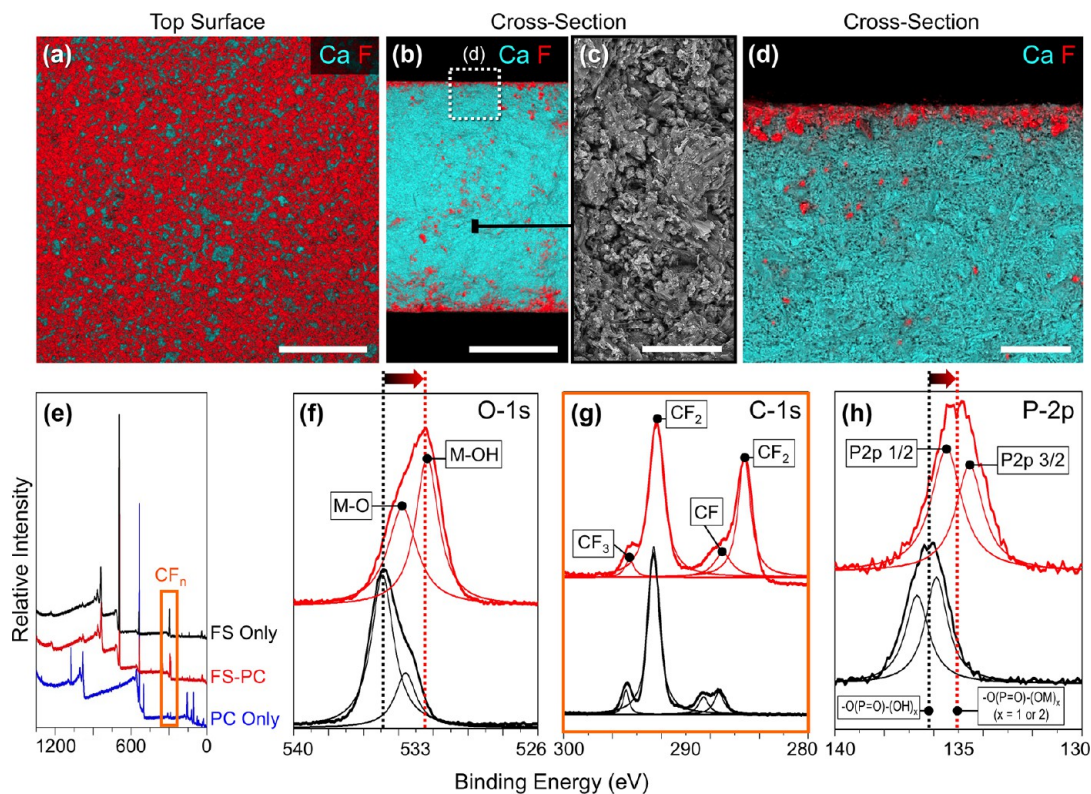


Figure 3. Chemical composition analysis of LIB-PC. (a–d) EDS elemental map of the surface (a) and cross-section (b and d) of modified PC. Chemical modification by the fluorosurfactant (F, red) uniformly coats the surface but does not completely permeate the bulk material (Ca, cyan), instead forming a chemically modified zone near the surface. (c) Porous structure of cement viewed under high magnification scanning electron microscopy. Scale bar for a and b is 1 mm, for c is 40 μm , and for d is 100 μm . (e–h) XPS spectra, including (e) survey and narrow scans of (f) O 1s, (g) C 1s, and (h) P 2p peaks of free fluorosurfactant (black), fluorosurfactant-modified PC (red), and untreated PC (blue) demonstrating that there are chemically bound fluorosurfactant molecules (as indicated by the shift shown by the arrows) on the surface of modified PC.

new hybrid material exhibits durability against environmental challenges such as moisture, acids, and ions while maintaining inherent mechanical properties critical for structural materials. Unlike conventional repellent surfaces, such as superhydrophobic surfaces and slippery liquid-infused porous surfaces (SLIPS), which are limited to mainly surface effects, our approach not only achieves surface repellency but also uses a mobile liquid phase to block unwanted materials from entering the bulk of the porous solid (Figure 1b).¹³ As a result, the permeability of a LIB prepared using Portland cement (LIB-PC) is significantly reduced without compromising its inherent mechanical properties. We demonstrate the feasibility of LIB for real-world applications using industry standard methods such as acid resistance, chloride-ion penetrability, and freeze–thaw cycling.^{61–63} These results suggest that LIB can be further developed as a stand-alone treatment or as a complement to other existing surface treatments to improve the long-term protection of cementitious materials.

2. RESULTS AND DISCUSSION

2.1. Introducing LIB into Portland Cement (PC).

Portland cement (PC) samples were prepared according to the manufacturer's guidelines (see Experimental Section for additional details). The samples were modified with a fluoroaliphatic phosphate ester (MASURF FS-100, hereafter referred to as “fluorosurfactant” or “FS”). The modified PC was then infused with a fluorinated oil (Krytox PFPE GPL 100, hereafter referred to as “K100”) to form a liquid barrier (LIB-PC) (Figure 2a). Extensive characterization of the chemical

composition and uniformity of LIB-PC was performed using energy-dispersive spectroscopy (EDS), X-ray photoelectron spectroscopy (XPS), and Fourier transform infrared spectroscopy (FT-IR). The presence of a porous network and the pore size distribution within the bulk of modified PC was confirmed by cross-sectional SEM (Figure 3c) and N₂ adsorption–desorption experiments (Figure S1, Table S1). Qualitative elemental mapping using EDS revealed a relatively uniform surface coating of fluorosurfactant with fluorine concentration decreasing from the surface to the bulk (Figure 3a–d). Effective chemical binding of the fluorosurfactant to the surface was confirmed by XPS (Figure 3e–h). The peaks from F 1s (~ 693 – 695 eV) and C 1s (~ 280 – 300 eV) corresponding to CF₂ and CF₃ are observed on PC only after modifying with fluorosurfactant. The initially high binding O 1s peak from unbound fluorosurfactant, $-\text{O}(\text{P}=\text{O})-(\text{OH})_x$ (~ 531 – 539 eV), shifts to low binding energy upon binding with the surface metal (M), $-\text{O}(\text{P}=\text{O})-(\text{OM})_x$ (~ 530 – 537 eV), where $x = 1$ or 2 , and is also convoluted with the signals due to the metal hydroxide and metal oxide present on the surface of PC. The shift in peaks in the P 2p region confirms a change in the binding energy of the functional phosphate group on the fluorosurfactant from unbound, $-\text{O}(\text{P}=\text{O})-(\text{OH})_x$ to bound in the form of a phosphate ester with a metal (M), $-\text{O}(\text{P}=\text{O})-(\text{OM})_x$, where $x = 1$ or 2 (Figure 2a). This layer of bound fluorosurfactant concentrated near the surface has a higher chemical affinity for K100 than does the bulk material. When combined with the 3D interconnected porous structure (Figure 3c), this enables the transport of K100 from the bulk and its replenishment on a

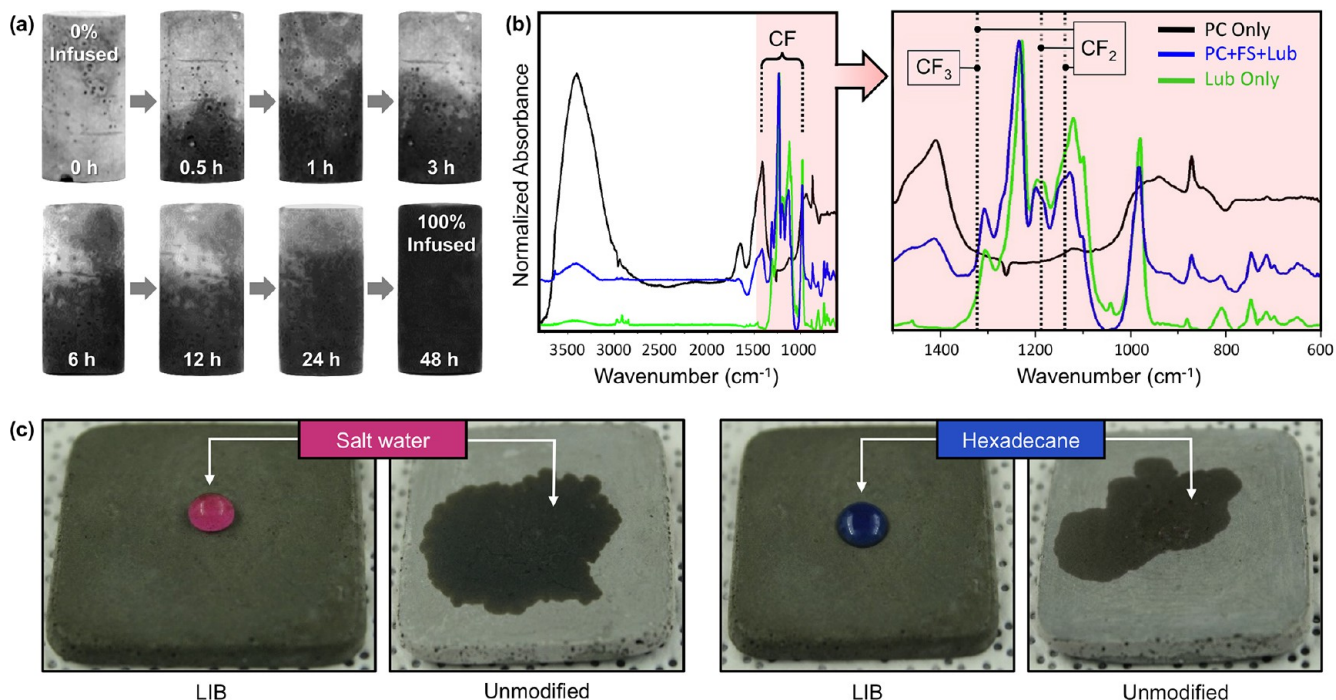


Figure 4. Formation of LIB through lubricant infiltration and its effect on decreasing liquid contaminant penetration. (a) Time-lapse images of a cylindrical modified PC sample ($\phi = 1$ cm, $h = 2$ cm) undergoing lubricant (K100) infiltration. Progression of infiltration can be monitored visually as the cement sample turns darker with increasing infiltration time. (b) After 48 h infiltration, the horizontal cross-section of the sample was characterized using FT-IR to confirm that the liquid component has fully penetrated the sample. Cross-section of an untreated PC sample was used as a control. (c) LIB formed by lubricant infiltration decreases permeability of the cement by various liquids, including salt water and hexadecane, while untreated PC displayed undesired absorption within seconds. Each sample measures ca. 4 cm \times 4 cm.

damaged surface, in contrast to most liquid-infused 2D surfaces that merely retain liquid due to a limited liquid reservoir in the interfacial layer. To confirm the mobility of the K100 within the bulk, modified PC cylindrical samples ($\phi = 1$ cm, height = 2 cm) were allowed to sit in a thin pool of K100 (Figure 4a). As a result of capillary rise through the porous network, K100 was able to fully penetrate the sample within 48 h (0.4 mm h^{-1}). Note that the capillary length (l_c) of Krytox is ~ 1 mm, meaning capillary forces will dominate over gravitational forces when the pore sizes are < 1 mm, as is the case here.⁶⁴ The permeation of K100 throughout the bulk of the modified PC was confirmed visually by the progressive darkening of the samples over time (Figure 4a) and by FT-IR spectroscopy measurements of the horizontal cross sections taken near the center of the samples (Figure 4b). As compared to untreated PC, K100 shows unique infrared absorption bands corresponding to the $-CF$ stretching mode (strong) between 1000 and 1400 cm^{-1} , specifically the $-CF_2$ symmetric stretching mode (1149 cm^{-1} , 1199 cm^{-1} , 1300 cm^{-1}) and the $-CF_3$ stretching mode (1300 cm^{-1}). These peaks were observed in the cross-section measurements of the samples after infusion with K100. In addition to the liquid retained within the bulk, the ability of the porous structure to maintain a stable liquid barrier layer at the surface was confirmed by testing its repellency against salt water and hexadecane. As compared to untreated PC samples, where liquid contaminants were readily absorbed, LIB-PC effectively repels both of these liquids (Figure 4c, Table 1).

Though the primary focus of this discussion is the application of LIB to PC, we confirmed by parallel studies that LIB can also be applied to alternative cement binders such as geopolymers (Figures S2–S4, Tables S2 and S3).

Table 1. LIB-PC Repellency against Liquids with Different Surface Tensions Characterized by the Sliding Angle

liquid	surface tension ($mN m^{-1}$) at $20^\circ C$	sliding angle (deg)
<i>n</i> -hexadecane	20.2	14 ± 4
ethanol	22.1	13 ± 3
salt water (3.5% wt)	72.8	10 ± 2

2.2. Surface Wetting Properties. To verify the surface repellency of LIB-PC, we measured the static contact angle (CA), contact angle hysteresis (CAH), and sliding angle (SA) of water. Though the CA of water on modified PC was high ($\sim 150^\circ$), the majority of droplets were pinned even at a tilt angle of 90° , resembling the “Rose petal effect” (where a water droplet placed on the surface retains its spherical shape but does not roll even when the sample is inverted).^{24,67} This behavior is attributed to the inherent heterogeneous porosity of the cement causing a Wenzel-like wetting state. Thus, cementitious materials can be rendered highly hydrophobic by reducing their surface energy with fluorosurfactants; however, the resulting material does not show low roll-off angles as observed on superhydrophobic surfaces. As a result, these pinned droplets dynamically wet the surface over time. In contrast, LIB-PC maintained a stable layer of K100 on the surface and displayed omniphobic properties with low SA (Table 1) and minimal pinning of water droplets. Untreated PC displayed instantaneous absorption upon application of various liquids (e.g., salt water or hexadecane) (Figure 4c). As such, the substrate–lubricant interface in LIB-PC remains stable and is not perturbed when another immiscible liquid is applied to the surface.

2.3. Mechanical Properties. Introduction of the LIB does not negatively affect the inherent bulk mechanical properties of Portland cement (Table 2), which are essential for applications

Table 2. Mechanical Testing of Untreated PC and LIB-PC

sample	Young's modulus (GPa)	compressive strength (MPa)
untreated PC	1.21 ± 0.29	19.9 ± 3.1
LIB-PC	1.23 ± 0.23	17.3 ± 3.3

requiring structural stability. The Young's modulus of LIB-PC remained unchanged compared to PC, and there was only a very slight reduction in compressive strength. To assess the durability of the LIB treatment, LIB-PC was subjected to mechanical wear testing (sand-drop test, ASTM D968-17) using yttria-stabilized zirconia beads with diameters varying from 0.8 to 2 mm. LIB-PC maintained a high CA and low CAH after application of a high impinging energy of $>5.0 \text{ kJ m}^{-2}$ (Figure 5). In contrast, a commercially available spray-on superhydrophobic coating (NeverWet coating) applied to the surface of PC was severely damaged, to the point of not yielding measurable CAH, after application of just $1.520 \pm 0.005 \text{ kJ m}^{-2}$ of impinging energy. Continuous testing showed that just $4.527 \pm 0.013 \text{ kJ m}^{-2}$ of impinging energy was sufficient to abrasively remove the NeverWet coating, allowing water to permeate into the underlying cement (Figure 5). Parallel studies showed that application of LIB to geopolymers did not negatively impact their mechanical properties (Figure S5), and their wetting properties (CA and CAH) were maintained after sand abrasion testing (Figure S6). The high tolerance of LIB-PC for wear and abrasion was further demonstrated by the fact that liquid droplets maintained their original sliding angle after the surface was abraded with a razor blade, 3000-grit sandpaper, and a flat head screw driver (Figure 6, Movies S1 and S2). Post abrasion surface visualization revealed spontaneous migration of the lubricant to the damaged sites due to the high chemical affinity of K100 for the concentrated layer of fluorosurfactant, affording LIB-PC a unique self-healing capability.

2.4. Barrier Properties. The ability of LIB-PC to mitigate deterioration from exposure to weathering conditions was also examined using a series of industry standard tests including acid resistance (ASTM C267, see SI for details), chloride-ion penetrability (ASTM C1202, Figure S7, see SI for details),

and freeze–thaw cyclability (ASTM C1262) (Figure 7, see SI for details). All of these tests demonstrated that LIB-PC significantly reduced the penetration of different ionic species into the cement. For example, after submersion in a solution of 1 wt % hydrochloric acid for 7 days, LIB-PC had a reduced mass loss rate (2.5 mg h^{-1}) and had minor color changes on the edges. Untreated PC had a significantly higher mass loss rate (8.9 mg h^{-1}) and an appreciable color change indicative of corrosion (Figure 7a and 7b). The large difference in mass loss rates and color change can be attributed to the alkaline nature of untreated PC, making it highly susceptible to acid attacks. Once penetrated, acids will readily react with the hydration products (produced in formation of PC) to form insoluble salts and corrosion byproducts (e.g., hydrous silicon dioxide, iron oxide, and aluminum hydroxide). The insoluble salts are swiftly removed through diffusion, and the corrosion byproducts remain in a now weakened cement structure.^{65–67} In contrast, LIB-PC prevents acid penetration and thereby inhibits the degradation process.

To further confirm the stability of the liquid phase within LIB-PC, we measured the ion penetrability after subjecting samples ($\phi = 2 \text{ cm}$, $h = 1 \text{ cm}$) to freeze–thaw cycling (Figure 7c and 7d). A set of line defects (1 cm long) on the surface was deliberately introduced on each sample via laser etching (see Figure 7c) to create stress points for failure. We observed new cracks around the engraved defects of the untreated PC (Figure 7c, left) after only two freeze–thaw cycles, while none were observed on the LIB-PC (Figure 7c, right). The ion penetration is an indirect measurement for water uptake. Due to the much lower freezing point ($-55 \text{ }^\circ\text{C}$) than that of water, the mobile phase remains as a liquid at lower temperatures and effectively blocks water from entering to the porous bulk. As a result, the mechanical damage of the cement due to the volume expansion of freezing water can be effectively minimized. After each subsequent freeze–thaw cycle, the chloride-ion penetrability of the LIB-PC was maintained at nearly zero, while that of the untreated PC showed a significant increase after each cycle with clear surface deterioration (Figure 7d). LIB not only protects the integrity of the cement by mitigating the formation of cracks, but also corrosion prone reinforcements (e.g., re-bar) typically contained within the cement matrix. Additionally, surface ice mitigation is another potential benefit.

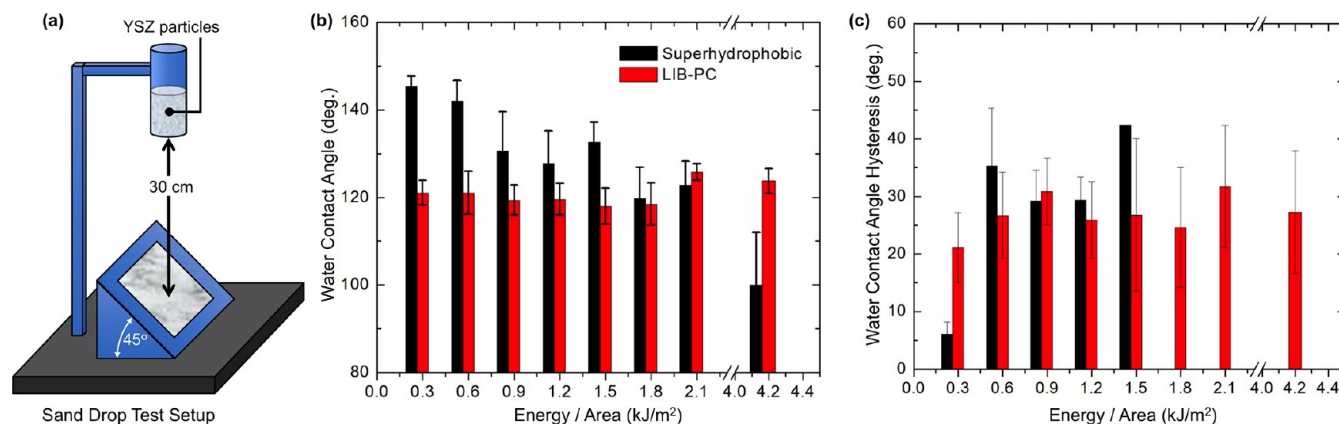


Figure 5. Mechanical wear resistance of LIB-PC versus a superhydrophobic surface (NeverWet coating). (a) Schematic of the sand-drop test setup adapted from ASTM D968-17 used to compare LIB-PC and NeverWet. Water CA (b) and CAH (c) of samples after sand abrasion testing to compare LIB-PC to NeverWet. Note that after application of just $1.520 \pm 0.005 \text{ kJ m}^{-2}$ of impinging energy, NeverWet was sufficiently damaged to the point of not yielding measurable CAH.

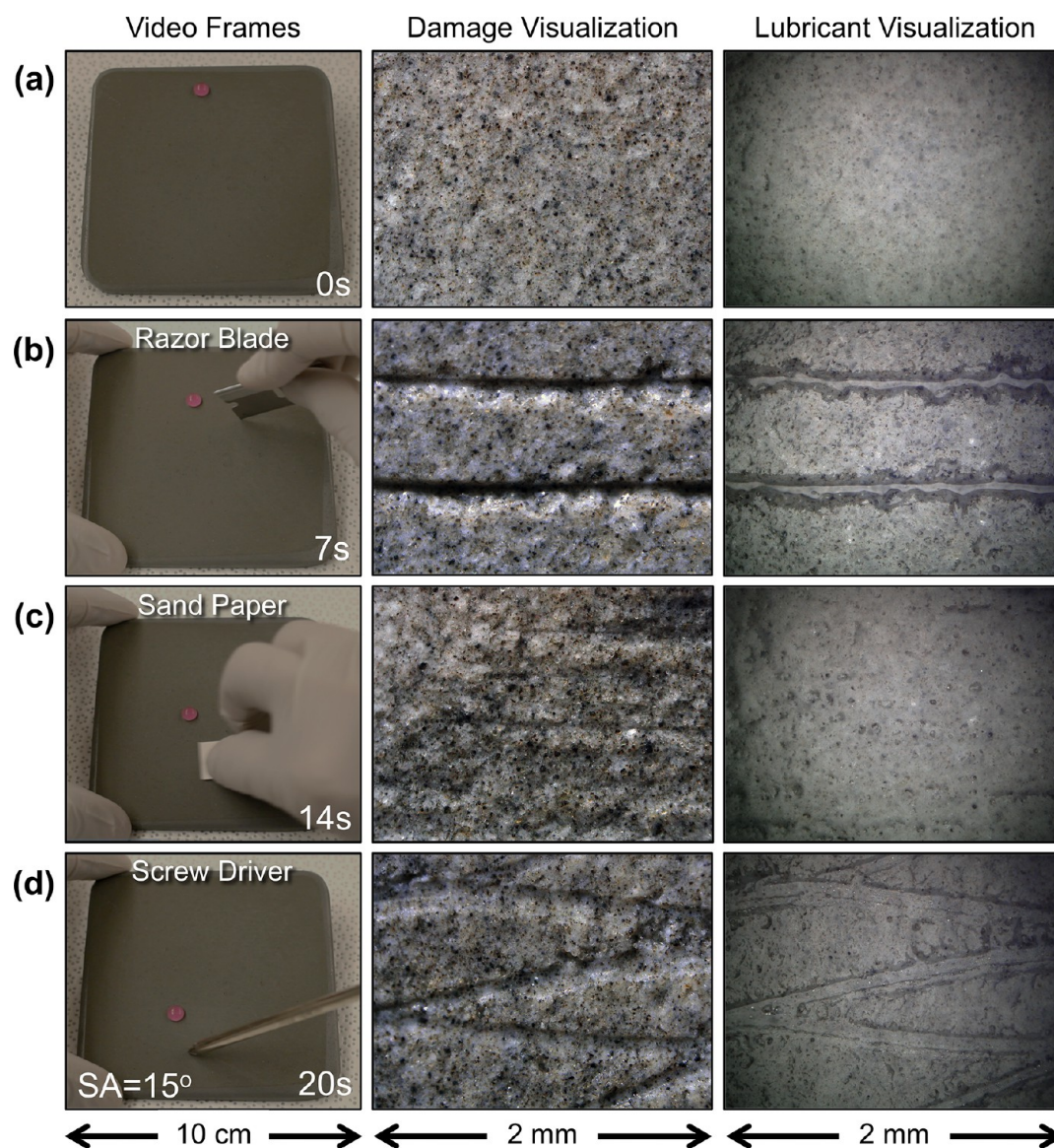


Figure 6. Uncompromised wetting properties of LIB-PC after significant mechanical damage. (Left) Still images from [Movie S2](#), showing various mechanical abrasion tests. (Middle) Bright-field optical micrographs of the underlying cement surface subjected to various abrasion mechanisms. (Right) Polarized optical micrographs for lubricant visualization obtained shortly after induction of mechanical damage. (a) Original, undamaged surface of LIB-PC. (b) LIB-PC damaged with a razor blade; width of the defects is 10–20 μm . (c) LIB-PC abraded with silicon carbide sandpaper (grit size 3000). Abrasion removed approximately 10–15 μm of material from the surface (as observed by change in focal plane), and the LIB is still present. (d) LIB-PC scratched with a screwdriver; width of the defects is 30–50 μm .

2.5. Protection from Biofouling. We used a green algal species (*Chlamydomonas reinhardtii*) to test the ability of LIB-PC to resist biofouling. Stock solutions of nonaxenic *C. reinhardtii*, (UTEX no. 89) from the University of Texas Culture Collection were grown in Bristol Medium over a period of 7 days. The stock solution was then diluted at a ratio of 1:8, stock culture to fresh media. The LIB-PC and untreated PC (3 replicates each) were introduced into square Petri dishes that were then filled with 80 mL of algal culture solution. Cultures were incubated under a set of Sun Blaze TSHO fluorescent light fixtures (Sunlight Supply, Inc., Vancouver, WA). The lamps were on timers to provide 16 h of light followed by 8 h of dark. The temperature of the culture media was kept at 25 $^{\circ}\text{C}$, and after 7 days of biofilm growth the treatments were lifted out of the culture medium at a controlled rate of 0.5 mm/s. Once the

substrate was completely clear of the medium, it was photographed for image analysis of the biofilm coverage.

The release of the highly alkaline byproducts from the bulk of the untreated PC samples increased the local pH (pH = 12) of the growth medium, inhibiting algal growth. In contrast, the excellent barrier properties of LIB-PC almost entirely prevented penetration of external species and outward diffusion of alkaline species. Accordingly, LIB-PC shows no toxicity against algal biofilm and allows for biofilm formation. Simple withdrawal of the sample from the medium showed excellent biofilm removal from the LIB-PC surface ([Figure 8](#)), confirming the nonadhesive character of LIB.

3. CONCLUSIONS

We demonstrated that a self-repairing hybrid liquid-in-solid protective barrier can be employed on PC and other

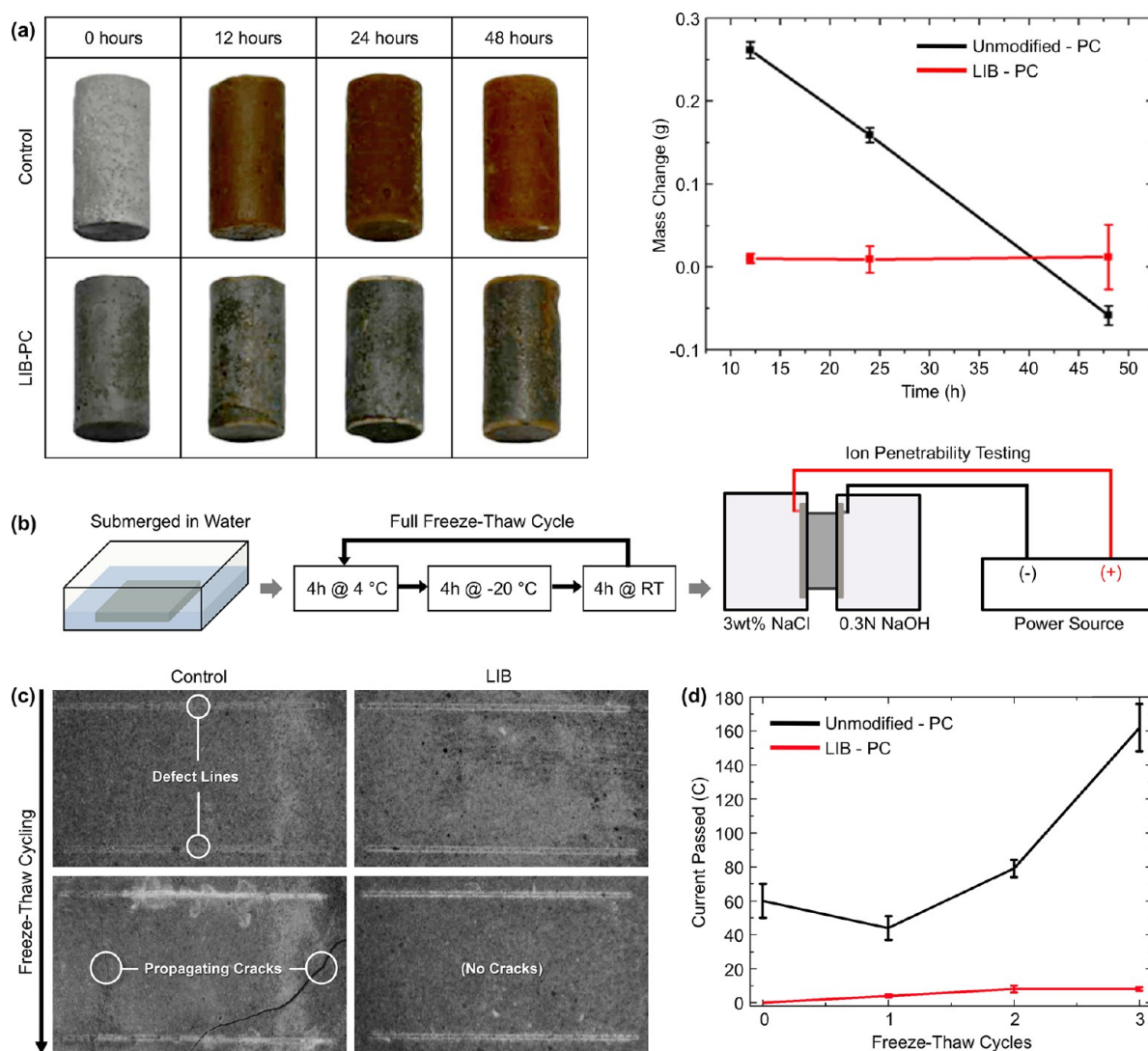


Figure 7. Characterization of deterioration from exposure to weathering conditions of the LIB-PC and untreated PC. (a) Acid resistance test. (Left) Photographs of cement samples at different time points, clearly demonstrating appreciable surface oxidation (orange) in the control samples. (Right) Mass loss upon acid exposure over time. Initial increase in mass from the control samples (untreated PC at 12 h) was due to absorption of the acid solution. (b) Schematics of freeze–thaw and chloride-ion penetrability cyclical testing. (c) Optical micrographs of untreated PC (left) and LIB-PC (right) during freeze–thaw testing cycles with intentional line defects. Untreated PC showed crack propagation through the sample, whereas there were no visible new cracks on the LIB-PC surfaces. (d) Measured chloride-ion penetrability of LIB-PC and PC control after each freeze–thaw cycle.

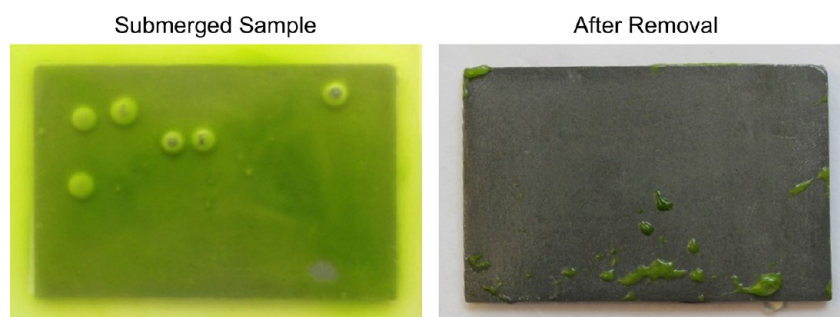


Figure 8. Foul-release and toxicity testing of LIB-PC with *C. reinhardtii*. Healthy growth of the algae in the presence of LIB-PC indicates minimal seepage of alkaline species, and ease with which the biofilm was removed indicates the superior nonadhesive properties of LIB-PC.

cementitious materials such as geopolymers to reduce the permeability of the bulk material to moisture and ions while maintaining the mechanical properties (Young's modulus and compressive strength). Through industry standard tests we

show that the enhanced barrier function of LIB improves damage tolerance in abrasive environments and prevents infiltration of corrosive liquids, thereby significantly reducing degradation.

Most liquid-infused 2D surfaces that merely retain liquid due to a limited reservoir in the interfacial layer, LIB derives its unique strength from the dynamic nature of liquids trapped within the bulk of the micro–nanoporous solid. Specifically, LIB can reconfigure itself to cover and protect the surface against penetration of contaminants and physical damage due to the dominant role played by capillarity and interfacial energy in maintaining the stability and diffusion of entrapped liquids. Similarly, the dynamic properties of liquids have been used successfully in other micro-nanoscale systems, such as mechano-responsive switching of wetting properties and the gated permeability of porous membranes,^{18,25} spontaneous and reversible wicking of liquids to dynamically switch structural color in ordered porous systems,^{68,69} optofluidics,^{70,71} and microfluidic systems.⁷² In all cases, optimal performance of these hybrid materials requires careful selection of liquid and solid components.

The dynamic nature of solid-confined liquids such as LIB provides several critical advantages: (i) liquids can provide a self-repairing mechanism against mechanical damage, for example, by spontaneously filling and wetting into newly formed cracks; (ii) mobile liquid phase provides enhanced barrier properties against vapors by spontaneously sealing newly formed pores; (iii) displacement of air within a composite porous material by liquids of different refractive indices can offer a reliable visual indicator of system efficacy; (iv) a mobile liquid-phase component in hybrid composite systems can behave as a new transducer responding to environmental changes or designed cues (mechanical strain, pressure, temperature, and surface energy). This study provides a stepping stone for future designs of dynamically functioning porous materials that can be considered for applications such as prevention of microbial fouling within a rigid porous structure (e.g., biocompatible cements such as calcium phosphate or hydroxyapatite), prolongment of service life in corrosion-prone environments (e.g., marine structures and sewage systems), and limiting seepage of pollutants from toxic porous materials (e.g., porous metals).

EXPERIMENTAL SECTION

3.1. Preparation of Portland Cement. General type I/II PC (Ashgrove Cement Co.) paste mixtures were prepared by adding water to the dry cement at a ratio of 1:0.437 by weight. The pastes were mixed using a planetary mixer (Thinky Mixer ARE-310, Thinky USA) for 180 s at 600 rpm. Specimens were cast and sealed in silicone molds using parafilm. The samples were oven cured at 40 °C and ambient pressure for 24 h (see SI for the preparation of LIB-GP).

3.2. Chemical Modification and Lubrication. All of the chemicals are commercially available and used as received without further purification. Fluoroaliphatic phosphate ester (MASURF FS-100, see the chemical structure in Figure 2a) was supplied by Mason Surfactant (acquired by Pilot Chemicals). The fluorosurfactant solutions were prepared using reagent-grade ethanol. The liquid used to infuse the samples was Krytox GPL 100 (Chemours) after modification with the fluorosurfactant.

PC samples were functionalized in a stagnant 1 wt % fluorosurfactant solution in 95:5 v/v ethanol:water for 12 h at 70 °C and then placed in ethanol at 70 °C for 10 min to remove any residue present. The samples were then dried for 1–2 h at 70 °C to completely remove any remaining ethanol from the pores of the samples.

K100 lubricant was dispensed onto the surface of the samples. Depending on the sample size, the time to reach full lubrication took approximately 72 h or less.

Prepared samples were subjected to acid-resistance testing (ASTM C267), chloride-ion penetrability (ASTM C1202), freeze–thaw

cyclability (ASTM C1262), and biofouling testing. For all tests, the samples were prepared according to the procedures outlined above. The test methods used are described in the Supporting Information.

3.3. Characterization Methods. Energy-dispersive spectroscopy (EDS) was performed using a dual Bruker Xflash 5030 X-ray detector system on a Tescan (Brno, Czech Republic) Vega GMU scanning electron microscope. Chemical surface modification was confirmed using a Thermo Scientific K-Alpha X-ray photoelectron spectrometer (XPS). Multipoint, high-resolution, and depth-profiling scans were performed to obtain relevant spectra. Optical imaging was performed using a Keyence VHX-6000.

Compression tests were performed using an Instron 5566 Universal Testing Machine. Cylindrical specimens were prepared with a 10 mm diameter and 20 mm length, maintaining an aspect ratio of 2:1. Prior to testing, the sample ends were polished flat. All of the samples for the mechanical testing were prepared within the same batch and sealed in a closed container until they were tested.

The wetting properties of the samples were measured using a Krüss goniometer (model 590). Static water contact angles (8 μ L droplet) and contact angle hysteresis were determined using the built-in tangential regression model (“Tangent 2”). The SA measurements were performed using 20 μ L droplets.

The cross sections for FT-IR were prepared by horizontally cutting cylindrical molded samples ($\phi = 1$ cm, $h = 2$ cm) near the center using a slow-speed diamond saw. FT-IR measurements were performed on the cut edge of the cylindrical samples close to the center using a Bruker HYPERION 3000 FT-IR Microscope/VERTEX 70 FT-IR Spectrometer and an attenuated total reflectance objective with a germanium crystal. Measurements were carried out with a spectral resolution of 4 cm^{-1} on 64 background and sample scans in the range of 600–4000 cm^{-1} .

ASSOCIATED CONTENT

Supporting Information

The Supporting Information is available free of charge at <https://pubs.acs.org/doi/10.1021/acsami.0c06357>.

Pore size distribution calculated from N_2 adsorption–desorption isotherms using the Barrett, Joyner, and Halenda (BJH) method; pore size distribution of geopolymer samples prepared; EDS and XPS characterization performed on geopolymers; repellency against different liquids on LIB-GP; mechanical testing performed on geopolymers including compression testing and sand-drop testing; setup for the chloride-ion penetrability test (PDF)

Screwdriver abrasion on LIB-PC (MOV)

Different types of abrasion on LIB-PC (MOV)

AUTHOR INFORMATION

Corresponding Authors

Joanna Aizenberg – Wyss Institute for Biologically Inspired Engineering, John A. Paulson School of Engineering and Applied Sciences, and Department of Chemistry and Chemical Biology, Harvard University, Cambridge, Massachusetts 02138, United States; Email: jaiz@seas.harvard.edu

Philseok Kim – Wyss Institute for Biologically Inspired Engineering, Harvard University, Cambridge, Massachusetts 02138, United States; orcid.org/0000-0001-5814-2675; Email: philseok.kim@gmail.com

Authors

Gurminder K. Paink – Wyss Institute for Biologically Inspired Engineering, Harvard University, Cambridge, Massachusetts 02138, United States

Stefan Kolle – John A. Paulson School of Engineering and Applied Sciences, Harvard University, Cambridge, Massachusetts 02138, United States

Duy Le – Wyss Institute for Biologically Inspired Engineering, Harvard University, Cambridge, Massachusetts 02138, United States

James C. Weaver – Wyss Institute for Biologically Inspired Engineering, Harvard University, Cambridge, Massachusetts 02138, United States

Jack Alvarenga – Wyss Institute for Biologically Inspired Engineering, Harvard University, Cambridge, Massachusetts 02138, United States

Onyemaechi Ahanotu – Wyss Institute for Biologically Inspired Engineering, Harvard University, Cambridge, Massachusetts 02138, United States

Complete contact information is available at:

<https://pubs.acs.org/10.1021/acsami.0c06357>

Author Contributions

P.K. conceived the hybrid liquid-in-solid protective barrier concept. P.K. and G.P. designed and carried out the experimentation. S.K. carried out the biofouling experiments. D.L. assisted with industry standard tests. J.A. and O.A. assisted with characterization and method development of tests. J.W. collected the EDS and SEM data. J.A. and P.K. supervised the research. The manuscript was written through the contributions of all authors. All authors have given approval to the final version of the manuscript.

Funding

This work was in part supported by the Office of Naval Research (N00014-17-1-2913).

Notes

The authors declare no competing financial interest.

ACKNOWLEDGMENTS

We thank Tom Blough, Dr. Alexander Tesler, Richard Crowley, Alexander Vena, Alexander Lopatin, and Dr. Michael Aizenberg for discussions and Sydney Stenquist for assistance with antifouling experiments.

REFERENCES

- (1) Kosmatka, S. H.; Kerkhoff, B.; Panarese, W. C. *Design and Control of Concrete Mixtures*; Portland Cement Association: Skokie, IL, 2003.
- (2) Majidi, B. Geopolymer Technology, from Fundamentals to Advanced Applications: A Review. *Mater. Technol.* **2009**, *24* (2), 79–87.
- (3) Lecomte, I.; Henrist, C.; Liégeois, M.; Maseri, F.; Rulmont, a.; Cloots, R. (Micro)-Structural Comparison between Geopolymers, Alkali-Activated Slag Cement and Portland Cement. *J. Eur. Ceram. Soc.* **2006**, *26* (16), 3789–3797.
- (4) Khale, D.; Chaudhary, R. Mechanism of Geopolymerization and Factors Influencing Its Development: A Review. *J. Mater. Sci.* **2007**, *42* (3), 729–746.
- (5) De Belie, N. Microorganisms versus Stony Materials: A Love–Hate Relationship. *Mater. Struct.* **2010**, *43* (9), 1191–1202.
- (6) Venkatesan, P.; Palaniswamy, N.; Rajagopal, K. Corrosion Performance of Coated Reinforcing Bars Embedded in Concrete and Exposed to Natural Marine Environment. *Prog. Org. Coat.* **2006**, *56* (1), 8–12.
- (7) Kamaitis, Z. Structural Design of Polymer Protective Coatings for Reinforced Concrete Structures. Part I: Theoretical Considerations. *J. Civ. Eng. Manag.* **2007**, *13* (1), 11–17.

- (8) Kamaitis, Z. Structural Design of Polymer Protective Coatings for Reinforced Concrete Structures. Part II: Experimental Verification. *J. Civ. Eng. Manag.* **2007**, *13* (1), 19–26.

- (9) Cardenas, H. E. *Nanomaterials in concrete*; DEStech Publications: Lancaster, PA, 2012.

- (10) Kouloumbi, N.; Batis, G. Chloride Corrosion of Steel Rebars in Mortars with Fly Ash Admixtures. *Cem. Concr. Compos.* **1992**, *14* (3), 199–207.

- (11) Medeiros, M. H. F.; Castro-Borges, P.; Aleixo, D. M.; Quarcioni, V. a.; Marcondes, C. G. N.; Helene, P. Reducing Water and Chloride Penetration through Silicate Treatments for Concrete as a Mean to Control Corrosion Kinetics. *Int. J. Electrochem. Sci.* **2012**, *7* (10), 9668–9681.

- (12) Almusallam, a. a.; Khan, F. M.; Dulaijan, S. U.; Al-Amoudi, O. S. B. Effectiveness of Surface Coatings in Improving Concrete Durability. *Cem. Concr. Compos.* **2003**, *25* (4–5), 473–481.

- (13) Flores-Vivian, I.; Hejazi, V.; Kozhukhova, M. I.; Nosonovsky, M.; Sobolev, K. Self-Assembling Particle-Siloxane Coatings for Superhydrophobic Concrete. *ACS Appl. Mater. Interfaces* **2013**, *5* (24), 13284–13294.

- (14) Ramachandran, R.; Sobolev, K.; Nosonovsky, M. Dynamics of Droplet Impact on Hydrophobic/Icephobic Concrete with the Potential for Superhydrophobicity. *Langmuir* **2015**, *31* (4), 1437–1444.

- (15) Arabzadeh, A.; Ceylan, H.; Kim, S.; Gopalakrishnan, K.; Sassani, A.; Sundararajan, S.; Taylor, P. C. Superhydrophobic Coatings on Portland Cement Concrete Surfaces. *Constr. Build. Mater.* **2017**, *141*, 393–401.

- (16) Muhammad, N. Z.; Keyvanfar, A.; Muhd, M. Z.; Shafaghat, A.; Mirza, J. Waterproof Performance of Concrete: A Critical Review on Implemented Approaches. *Constr. Build. Mater.* **2015**, *101*, 80–90.

- (17) Wong, T. S.; Kang, S. H.; Tang, S. K.; Smythe, E. J.; Hatton, B. D.; Grinthal, A.; Aizenberg, J. Bioinspired Self-Repairing Slippery Surfaces with Pressure-Stable Omniphobicity. *Nature* **2011**, *477*, 443.

- (18) Hou, X.; Hu, Y.; Grinthal, A.; Khan, M.; Aizenberg, J. Liquid-Based Gating Mechanism with Tunable Multiphase Selectivity and Antifouling Behaviour. *Nature* **2015**, *519* (7541), 70–73.

- (19) Kim, P.; Kreder, M. J.; Alvarenga, J.; Aizenberg, J. Hierarchical or Not? Effect of the Length Scale and Hierarchy of the Surface Roughness on Omniphobicity of Lubricant-Infused Substrates. *Nano Lett.* **2013**, *13* (4), 1793–1799.

- (20) Shillingford, C.; MacCallum, N.; Wong, T.-S.; Kim, P.; Aizenberg, J. Fabrics Coated with Lubricated Nanostructures Display Robust Omniphobicity. *Nanotechnology* **2014**, *25* (1), 014019.

- (21) Sunny, S.; Vogel, N.; Howell, C.; Vu, T. L.; Aizenberg, J. Lubricant-Infused Nanoparticulate Coatings Assembled by Layer-by-Layer Deposition. *Adv. Funct. Mater.* **2014**, *24* (42), 6658–6667.

- (22) Howell, C.; Vu, T. L.; Lin, J. J.; Kolle, S.; Juthani, N.; Watson, E.; Weaver, J. C.; Alvarenga, J.; Aizenberg, J. Self-Replenishing Vascularized Fouling-Release Surfaces. *ACS Appl. Mater. Interfaces* **2014**, *6* (15), 13299–13307.

- (23) Tesler, A. B.; Kim, P.; Kolle, S.; Howell, C.; Ahanotu, O.; Aizenberg, J. Extremely Durable Biofouling-Resistant Metallic Surfaces Based on Electrodeposited Nanoporous Tungstite Films on Steel. *Nat. Commun.* **2015**, *6*, 8649.

- (24) Vogel, N.; Belisle, R. a; Hatton, B.; Wong, T.-S.; Aizenberg, J. Transparency and Damage Tolerance of Patternable Omniphobic Lubricated Surfaces Based on Inverse Colloidal Monolayers. *Nat. Commun.* **2013**, *4*, 2167.

- (25) Yao, X.; Hu, Y.; Grinthal, A.; Wong, T.-S.; Mahadevan, L.; Aizenberg, J. Adaptive Fluid-Infused Porous Films with Tunable Transparency and Wettability. *Nat. Mater.* **2013**, *12*, 529.

- (26) Villegas, M.; Zhang, Y.; Abu Jarad, N.; Soleymani, L.; Didar, T. F. Liquid-Infused Surfaces: A Review of Theory, Design, and Applications. *ACS Nano* **2019**, *13* (8), 8517–8536.

- (27) Galvan, Y.; Phillips, K. R.; Haumann, M.; Wasserscheid, P.; Zarraga, R.; Vogel, N. Ionic-Liquid-Infused Nanostructures as Repellent Surfaces. *Langmuir* **2018**, *34* (23), 6894–6902.

- (28) Tonelli, M.; Peppou-Chapman, S.; Ridi, F.; Neto, C. Effect of Pore Size, Lubricant Viscosity, and Distribution on the Slippery Properties of Infused Cement Surfaces. *J. Phys. Chem. C* **2019**, *123* (5), 2987–2995.
- (29) Stamatopoulos, C.; Hemrle, J.; Wang, D.; Poulikakos, D. Exceptional Anti-Icing Performance of Self-Impregnating Slippery Surfaces. *ACS Appl. Mater. Interfaces* **2017**, *9* (11), 10233–10242.
- (30) Niemelä-Anttonen, H.; Koivuluoto, H.; Tuominen, M.; Teisala, H.; Juuti, P.; Haapanen, J.; Harra, J.; Stenroos, C.; Lahti, J.; Kuusipalo, J.; Mäkelä, J. M.; Vuoristo, P. Icephobicity of Slippery Liquid Infused Porous Surfaces under Multiple Freeze–Thaw and Ice Accretion–Detachment Cycles. *Adv. Mater. Interfaces* **2018**, *5* (20), 1800828.
- (31) Juuti, P.; Haapanen, J.; Stenroos, C.; Niemelä-Anttonen, H.; Harra, J.; Koivuluoto, H.; Teisala, H.; Lahti, J.; Tuominen, M.; Kuusipalo, J.; Vuoristo, P.; Mäkelä, J. M. Achieving a Slippery, Liquid-Infused Porous Surface with Anti-Icing Properties by Direct Deposition of Flame Synthesized Aerosol Nanoparticles on a Thermally Fragile Substrate. *Appl. Phys. Lett.* **2017**, *110* (16), 161603.
- (32) Kreder, M. J.; Alvarenga, J.; Kim, P.; Aizenberg, J. Design of Anti-Icing Surfaces: Smooth, Textured or Slippery? *Nat. Rev. Mater.* **2016**, *1* (1), 15003.
- (33) Irajizad, P.; Hasnain, M.; Farokhnia, N.; Sajadi, S. M.; Ghasemi, H. Magnetic Slippery Extreme Icephobic Surfaces. *Nat. Commun.* **2016**, *7* (1), 13395.
- (34) Golovin, K.; Dhyani, A.; Thouless, M. D.; Tuteja, A. Lowinterfacial Toughness Materials for Effective Large-Scale Deicing. *Science* **2019**, *364* (6438), 371–375.
- (35) Ma, L.; Zhang, Z.; Liu, Y.; Hu, H. An Experimental Study on the Durability of Icephobic Slippery Liquid-Infused Porous Surfaces (SLIPS) Pertinent to Aircraft Anti-/De-Icing. *2018 Atmospheric and Space Environments Conference*, Atlanta, GA; American Institute of Aeronautics and Astronautics, 2018.
- (36) Wang, N.; Xiong, D.; Pan, S.; Wang, K.; Shi, Y.; Deng, Y. Robust Superhydrophobic Coating and the Anti-Icing Properties of Its Lubricants-Infused-Composite Surface under Condensing Condition. *New J. Chem.* **2017**, *41* (4), 1846–1853.
- (37) Yeong, Y. H.; Milonion, A.; Loth, E.; Sokhey, J. Self-Lubricating Icephobic Elastomer Coating (SLIC) for Ultralow Ice Adhesion with Enhanced Durability. *Cold Reg. Sci. Technol.* **2018**, *148*, 29–37.
- (38) Latthe, S. S.; Sutar, R. S.; Bhosale, A. K.; Nagappan, S.; Ha, C.-S.; Sadasivuni, K. K.; Liu, S.; Xing, R. Recent Developments in Air-Trapped Superhydrophobic and Liquid-Infused Slippery Surfaces for Anti-Icing Application. *Prog. Org. Coat.* **2019**, *137*, 105373.
- (39) Barthwal, S.; Lee, B.; Lim, S.-H. Fabrication of Robust and Durable Slippery Anti-Icing Coating on Textured Superhydrophobic Aluminum Surfaces with Infused Silicone Oil. *Appl. Surf. Sci.* **2019**, *496*, 143677.
- (40) Yeong, Y. H.; Milonion, A.; Loth, E.; Sokhey, J. Self-Lubricating Icephobic Elastomer Coating (SLIC) for Ultralow Ice Adhesion with Enhanced Durability. *Cold Reg. Sci. Technol.* **2018**, *148*, 29–37.
- (41) Yuan, S.; Li, Z.; Song, L.; Shi, H.; Luan, S.; Yin, J. Liquid-Infused Poly(styrene-*b*-isobutylene-*b*-styrene) Microfiber Coating Prevents Bacterial Attachment and Thrombosis. *ACS Appl. Mater. Interfaces* **2016**, *8* (33), 21214–21220.
- (42) Juthani, N.; Howell, C.; Ledoux, H.; Sotiri, I.; Kelso, S.; Kovalenko, Y.; Tajik, A.; Vu, T. L.; Lin, J. J.; Sutton, A.; Aizenberg, J. Infused Polymers for Cell Sheet Release. *Sci. Rep.* **2016**, *6*, 26109.
- (43) Sotiri, I.; Overton, J. C.; Waterhouse, A.; Howell, C. Immobilized Liquid Layers: A New Approach to Anti-Adhesion Surfaces for Medical Applications. *Exp. Biol. Med.* **2016**, *241* (9), 909–918.
- (44) Kovalenko, Y.; Sotiri, I.; Timonen, J. V. I.; Overton, J. C.; Holmes, G.; Aizenberg, J.; Howell, C. Bacterial Interactions with Immobilized Liquid Layers. *Adv. Healthcare Mater.* **2017**, *6* (15), 1600948.
- (45) Wei, C.; Zhang, G.; Zhang, Q.; Zhan, X.; Chen, F. Silicone Oil-Infused Slippery Surfaces Based on Sol–Gel Process-Induced Nanocomposite Coatings: A Facile Approach to Highly Stable Bioinspired Surface for Biofouling Resistance. *ACS Appl. Mater. Interfaces* **2016**, *8* (50), 34810–34819.
- (46) Kratochvil, M. J.; Welsh, M. A.; Manna, U.; Ortiz, B. J.; Blackwell, H. E.; Lynn, D. M. Slippery Liquid-Infused Porous Surfaces That Prevent Bacterial Surface Fouling and Inhibit Virulence Phenotypes in Surrounding Planktonic Cells. *ACS Infect. Dis.* **2016**, *2* (7), 509–517.
- (47) Li, J.; Ueda, E.; Paulssen, D.; Levkin, P. A. Slippery Lubricant-Infused Surfaces: Properties and Emerging Applications. *Adv. Funct. Mater.* **2019**, *29* (4), 1802317.
- (48) Awad, T. S.; Asker, D.; Hatton, B. D. Food-Safe Modification of Stainless Steel Food-Processing Surfaces to Reduce Bacterial Biofilms. *ACS Appl. Mater. Interfaces* **2018**, *10* (27), 22902–22912.
- (49) Tenjimbayashi, M.; Park, J.-Y.; Muto, J.; Kobayashi, Y.; Yoshikawa, R.; Monnai, Y.; Shiratori, S. In Situ Formation of Slippery-Liquid-Infused Nanofibrous Surface for a Transparent Antifouling Endoscope Lens. *ACS Biomater. Sci. Eng.* **2018**, *4* (5), 1871–1879.
- (50) He, W.; Liu, P.; Zhang, J.; Yao, X. Emerging Applications of Bioinspired Slippery Surfaces in Biomedical Fields. *Chem. - Eur. J.* **2018**, *24* (56), 14864–14877.
- (51) Howell, C.; Grinthal, A.; Sunny, S.; Aizenberg, M.; Aizenberg, J. Designing Liquid-Infused Surfaces for Medical Applications: A Review. *Adv. Mater.* **2018**, *30* (50), 1802724.
- (52) Sunny, S.; Cheng, G.; Daniel, D.; Lo, P.; Ochoa, S.; Howell, C.; Vogel, N.; Majid, A.; Aizenberg, J. Transparent Antifouling Material for Improved Operative Field Visibility in Endoscopy. *Proc. Natl. Acad. Sci. U. S. A.* **2016**, *113* (42), 11676–11681.
- (53) Wang, P.; Zhang, D.; Sun, S.; Li, T.; Sun, Y. Fabrication of Slippery Lubricant-Infused Porous Surface with High Underwater Transparency for the Control of Marine Biofouling. *ACS Appl. Mater. Interfaces* **2017**, *9* (1), 972–982.
- (54) Ware, C. S.; Smith-Palmer, T.; Peppou-Chapman, S.; Scarratt, L. R. J.; Humphries, E. M.; Balzer, D.; Neto, C. Marine Antifouling Behavior of Lubricant-Infused Nanowrinkled Polymeric Surfaces. *ACS Appl. Mater. Interfaces* **2018**, *10* (4), 4173–4182.
- (55) Amini, S.; Kolle, S.; Petrone, L.; Ahanotu, O.; Sunny, S.; Santano, C. N.; Hoon, S.; Cohen, L.; Weaver, J. C.; Aizenberg, J.; et al. Preventing Mussel Adhesion Using Lubricant-Infused Materials. *Science* **2017**, *357* (6352), 668.
- (56) He, X.; Cao, P.; Tian, F.; Bai, X.; Yuan, C. Infused Configurations Induced by Structures Influence Stability and Antifouling Performance of Biomimetic Lubricant-Infused Surfaces. *Surf. Coat. Technol.* **2019**, *358*, 159–166.
- (57) Peppou-Chapman, S.; Neto, C. Mapping Depletion of Lubricant Films on Antibiofouling Wrinkled Slippery Surfaces. *ACS Appl. Mater. Interfaces* **2018**, *10* (39), 33669–33677.
- (58) Kimmins, K. M.; James, B. D.; Nguyen, M.-T.; Hatton, B. D.; Sone, E. D. Oil-Infused Silicone Prevents Zebra Mussel Adhesion. *ACS Appl. Bio Mater.* **2019**, *2* (12), 5841–5847.
- (59) Keller, N.; Bruchmann, J.; Sollich, T.; Richter, C.; Thelen, R.; Kotz, F.; Schwartz, T.; Helmer, D. E.; Rapp, B. Study of Biofilm Growth on Slippery Liquid-Infused Porous Surfaces Made from Fluoropor. *ACS Appl. Mater. Interfaces* **2019**, *11* (4), 4480–4487.
- (60) Vena, A.; Kolle, S.; Stafslien, S.; Aizenberg, J.; Kim, P. Self-Stratifying Porous Silicones with Enhanced Liquid Infusion and Protective Skin Layer for Biofouling Prevention. *Adv. Mater. Interfaces* **2020**, 2000359.
- (61) ASTM Standard C1262, *Evaluating the Freeze-Thaw Durability of Dry-Cast Segmental Retaining Wall Units and Related Concreted Units*; ASTM International: West Conshohocken, PA, 2010.
- (62) ASTM Standard C267, *Chemical Resistance of Mortars, Grouts, and Monolithic Surfacing and Polymer Concretes*; ASTM International: West Conshohocken, PA, 2012.
- (63) ASTM Standard C1202, *Electrical Indication of Concrete's Ability to Resist Chloride Ion Penetration*; ASTM International: West Conshohocken, PA, 2012.
- (64) Sun, J.; Weisensee, P. B. Microdroplet Self-Propulsion during Dropwise Condensation on Lubricant-Infused Surfaces. *Soft Matter* **2019**, *15* (24), 4808–4817.

(65) Pavlík, V. Corrosion of Hardened Cement Paste by Acetic and Nitric Acids Part I: Calculation of Corrosion Depth. *Cem. Concr. Res.* **1994**, *24* (3), 551–562.

(66) Delagrave, A.; Pigeon, M.; Marchand, J.; Revertégat, É. Influence of Chloride Ions and PH Level on the Durability of High Performance Cement Pastes (Part II). *Cem. Concr. Res.* **1996**, *26* (5), 749–760.

(67) Feng, L.; Zhang, Y.; Xi, J.; Zhu, Y.; Wang, N.; Xia, F.; Jiang, L. Petal Effect: A Superhydrophobic State with High Adhesive Force. *Langmuir* **2008**, *24* (8), 4114–4119.

(68) Burgess, I. B.; Mishchenko, L.; Hatton, B. D.; Kolle, M.; Lončar, M.; Aizenberg, J. Encoding Complex Wettability Patterns in Chemically Functionalized 3D Photonic Crystals. *J. Am. Chem. Soc.* **2011**, *133* (32), 12430–12432.

(69) Burgess, I. B.; Koay, N.; Raymond, K. P.; Kolle, M.; Lončar, M.; Aizenberg, J. Wetting in Color: Colorimetric Differentiation of Organic Liquids with High Selectivity. *ACS Nano* **2012**, *6* (2), 1427–1437.

(70) Kim, M.; Pan, M.; Gai, Y.; Pang, S.; Han, C.; Yang, C.; Tang, S. K. Y. Optofluidic Ultrahigh-Throughput Detection of Fluorescent Drops. *Lab Chip* **2015**, *15* (6), 1417–1423.

(71) Tang, S. K. Y.; Whitesides, G. M. Optical Components Based on Dynamic Liquid-Liquid Interfaces. In *Optofluidics: Fundamentals, Devices and Applications*; Fainman, Y., Lee, L. P., Psaltis, D., Yang, C., Eds.; McGraw-Hill: New York, 2010; pp 33–57.

(72) Selck, D. A.; Ismagilov, R. F. Instrument for Real-Time Digital Nucleic Acid Amplification on Custom Microfluidic Devices. *PLoS One* **2016**, *11* (10), e0163060.